REPORT DOCUMENTATION PAGE

Form Approved
OMB No. 0704-0188

Public reporting burden for this collection of information is estimated to average 1 hour per response, including the time for reviewing instructions, searching existing data sources, gathering and maintaining the data needed, and completing and reviewing this collection of information. Send comments regarding this burden estimate or any other aspect of this collection of information, including suggestions for reducing this burden to Department of Defense, Washington Headquarters Services, Directorate for Information Operations and Reports (0704-0188), 1215 Jefferson Davis Highway, Suite 1204, Arlington, VA 22202-4302. Respondents should be aware that notwithstanding any other provision of law, no person shall be subject to any penalty for failing to comply with a collection of information if it does not display a currently valid OMB control number. **PLEASE DO NOT RETURN YOUR FORM TO THE ABOVE ADDRESS.**

1. REPORT DATE *(DD-MM-YYYY)*	2. REPORT TYPE		3. DATES COVERED *(From - To)*
09-08-2005	Journal Article		

4. TITLE AND SUBTITLE

Nozzle Plume Impingement on Spacecraft Surfaces: Effects of Surface Roughness (POSTPRINT)

5a. CONTRACT NUMBER

5b. GRANT NUMBER

5c. PROGRAM ELEMENT NUMBER

6. AUTHOR(S)

C. Ngalande, T. Lilly, M. Killingsworth, & S. Gimelshein (UCLA);

A. Ketsdever (AFRL/PRSA)

5d. PROJECT NUMBER
50260568

5e. TASK NUMBER

5f. WORK UNIT NUMBER

7. PERFORMING ORGANIZATION NAME(S) AND ADDRESS(ES)

Air Force Research Laboratory (AFMC)
AFRL/PRSA
10 E. Saturn Blvd.
Edwards AFB CA 93524-7680

8. PERFORMING ORGANIZATION REPORT NUMBER

AFRL-PR-ED-JA-2005-306

9. SPONSORING / MONITORING AGENCY NAME(S) AND ADDRESS(ES)

Air Force Research Laboratory (AFMC)
AFRL/PRS
5 Pollux Drive
Edwards AFB CA 93524-70448

10. SPONSOR/MONITOR'S ACRONYM(S)

11. SPONSOR/MONITOR'S NUMBER(S)

AFRL-PR-ED-JA-2005-306

12. DISTRIBUTION / AVAILABILITY STATEMENT

Approved for public release; distribution unlimited (PA no. AFRL-ERS-PAS-2005-219).

13. SUPPLEMENTARY NOTES

14. ABSTRACT

An experimental and numerical effort was undertaken to assess the effects of a cold gas (T_0-300 K) nozzle plume impinging on simulated spacecraft surfaces. The nozzle flow impingement is investigated experimentally using a nano-Newton resolution force balance and numerically using the Direct Simulation Monte Carlo (DSMC) numerical technique. The Reynolds number range investigated in this study is from approximately 2 to 350 using nitrogen propellant. The thrust produced by the nozzle was first assessed on a force balance to provide a baseline case. Subsequently, aluminum plates were attached to the same force balance parallel to the plume flow to simulate spacecraft surfaces in proximity to the thruster. Three plates were used in this study, an electropolished plate with smooth surface, and two rough surface plates with equally spaced rectangular and triangular grooves. A 15% degradation in thrust was observed both experimentally and numerically for the plate relative to the free plume expansion case. The effect of surface roughness on thrust was found to be small due to molecules backscattered from the plate to the nozzle plenum wall. Additionally, the influence of surface roughness in the diverging part of the nozzle on thrust was examined numerically and found to be significant at Reynolds numbers less than 10.

15. SUBJECT TERMS

16. SECURITY CLASSIFICATION OF:			17. LIMITATION OF ABSTRACT	18. NUMBER OF PAGES	19a. NAME OF RESPONSIBLE PERSON
					Dr. Ingrid J. Wysong
a. REPORT	b. ABSTRACT	c. THIS PAGE	A	15	19b. TELEPHONE NUMBER *(include area code)*
Unclassified	**Unclassified**	**Unclassified**			(661) 275-5206

Standard Form 298 (Rev. 8-98)
Prescribed by ANSI Std. 239.18

AIAA 2005-5065

Nozzle Plume Impingement on Spacecraft Surfaces: Effects of Surface Roughness

C. Ngalande, M. Killingsworth, T. Lilly, and S. Gimelshein
University of Southern California, Los Angeles, CA 90089

A. Ketsdever
Air Force Research Laboratory, Edwards AFB, CA 93524

38th AIAA Thermophysics Conference
6-9 June 2005 / Toronto, Ontario, Canada

Nozzle Plume Impingement on Spacecraft Surfaces: Effects of Surface Roughness

C. Ngalande, M. Killingsworth, T. Lilly, and S. Gimelshein
University of Southern California, Los Angeles, CA 90089

A. Ketsdever
Air Force Research Laboratory, Propulsion Directorate, Edwards AFB, California 93524

Abstract

An experimental and numerical effort was undertaken to assess the effects of a cold gas (T_0=300 K) nozzle plume impinging on a simulated spacecraft surface. The nozzle flow impingement is investigated experimentally using a nano-Newton resolution force balance and numerically using the Direct Simulation Monte Carlo (DSMC) numerical technique. The Reynolds number range investigated in this study is from approximately 2 to 600 using nitrogen propellant. The thrust produced by the nozzle was first assessed on a force balance to provide a baseline case. Subsequently, aluminum plates were attached to the same force balance parallel to the plume flow. Three plates were used in this study, an electropolished plate with smooth surface, and two rough surface plates with equally spaced rectangular and triangular grooves. A 15% degradation in thrust was observed both experimentally and numerically for the plate relative to the free plume expansion case. The effect of surface roughness on thrust was found to be small due to molecules back scattered from the plate to the plenum wall. Additionally, the influence of surface roughness in the diverging part of the nozzle on nozzle thrust was examined numerically, and found to be significant at Reynolds numbers on the order or less than 10.

1 Introduction

When in orbit, spacecraft require on-board or secondary propulsion systems to perform orbit transfer, orbit maintenance, and attitude control maneuvers. An important issue in the use of any spacecraft propulsion system involves the assessment and reduction of effects caused by the interaction between the thruster plume and spacecraft surfaces [1]. Direct impingement of a thruster plume on surfaces can generate unwanted torques, localized surface heating, and surface contamination. Self impingement (i.e. the impingement of a thruster plume on a host satellite surface) generally occurs for small surface angles with respect to the propulsion system's thrust vector or occurs in the thruster backflow. Cross impingement (i.e. the impingement of one spacecraft's thruster plume onto another spacecraft) can occur at essentially any angle and is becoming increasingly important with the advent of microsatellite constellations. Many studies, both numerical [2]-[4] and experimental [5, 6], have been performed by various investigators to assess the impingement of plumes onto surfaces.

In recent years, micropropulsion systems have been developed to address the need for highly mobile microspacecraft. A wide array of concepts will require the expansion of propellant gases through microscale nozzles. Because many micropropulsion systems will also operate at relatively low pressures, the investigation of low Reynolds number flow has become increasingly important [7]. In the present study, an experimental and numerical effort has been developed to assess the effects of a nozzle plume impinging on a simulated spacecraft surface. Special attention is paid here to the impact of roughness on surface forces and flowfield structure.

The nozzle flow impingement is investigated experimentally using a nano-Newton resolution force balance and numerically using the Direct Simulation Monte Carlo (DSMC) numerical technique. The purpose of this work is to extend previous nozzle plume impingement results [5] to the low Reynolds number flow range for application to micropropulsion systems. The Reynolds number range investigated in this study is from 2 to approximately 600, based on the nozzle throat.

1

2 Experimental Setup

All thrust measurements were performed on the nano-Newton thrust stand (nNTS), which has been described in detail by Jamison et al.[8] The nNTS was installed in Chamber IV of the Collaborative High Altitude Flow Facilities (CHAFF-IV), which is a 3-m-diam 6-m-long cylindrical, high vacuum chamber. The facility was pumped with a 1-m-diam diffusion pump with a pumping speed of 25,000 L/s for molecular nitrogen. The ultimate facility pressure was approximately 10^{-6} torr with all operational pressures below 10^{-4} torr. A previous study [9] has shown that at these background pressures and corresponding thrust levels there is no evidence of background pressure effects on the thrust measurements in CHAFF-IV.

The conical De Laval nozzle used in this study is shown schematically in Fig. 1. The conical nozzle was scaled from the geometry used by Rothe [10]. The scaled Rothe geometry has a 30-deg subsonic section, a relatively sharp 1-mm-diam throat with radius of curvature rc = dt/4, a 20-deg diverging section, and an expansion ratio of 62.4. This geometry was selected because of the extensive experimental data that exists, which was previously used to verify the DSMC model's accuracy [11]. The nozzle was machined from aluminum and attached to a cylindrical aluminum plenum and mounted on the nNTS. Figure 2 shows a scanning electron microscope image of the nozzle side wall, where the surface features caused by the machining process are clearly evident. The effect of the rough diverging section walls on the nozzle's performance parameters will be investigated in the following sections.

After the free expansion thrust was measured, aluminum engineering surfaces with different surface roughness were attached to the thrust stand in the configuration shown in Fig. 1. The following three surfaces were used: (1) a electropolished flat surface (called smooth hereafter), (2) a surface with triangular (prism-like) grooves perpendicular to the plume axis, and (3) a surface with rectangular grooves perpendicular to the plume axis. The grooves are equally spaced, and the spacing is 0.005 m. The angle of triangular grooves is 90 deg, and the depth of rectangular grooves is the same as their thickness of 0.05 cm. The length of the plate (plume direction) is 3 cm, and the width is 3.81 cm. The grooves are made only in the region downstream from the nozzle exit plane (2.45 cm long).

The total force measured on the nNTS for this configuration is given by

$$F_{tot} = F_{th} - F_s + F_b \qquad (1)$$

where F_{th} is the thrust produced by the nozzle in the absence of the plate, F_s is the incident shear force on the plate (acting in the opposite direction as the thrust force), and F_b is the force exerted on the plenum wall due to gas pressure in the backflow. The angle of the plate was varied from 0 to 10 deg. The surface temperature was held constant throughout at 300 K.

The propellant was introduced to the plenum through an adjustable needle valve located downstream of a mass flowmeter. In the experimental configuration, the mass flowmeters were operated in the continuum regime throughout the pressure range investigated. The propellant used was molecular nitrogen. In this study, the stagnation pressures ranged from several about 0.1 torr to approximately 17 torr for both propellants, and the stagnation temperature was measured to be 300 K. The combination of stagnation pressure and temperature gave maximum Reynolds numbers of 350.

3 Numerical Method

Three geometric configurations have been considered in the computations. First, the nozzle expansion into a vacuum has been modeled. The experimental nozzle geometry has been used for for several stagnation pressures ranging from 18 to 1800 Pa. Second, the interaction of the nozzle plume with the inner part of a hollow cylinder aligned along the nozzle axis is modeled. The inner cylinder surface is considered as macroscopically smooth and rough with surface roughness specified as triangular and rectangular grooves perpendicular to the nozzle flow direction. The inner diameter of the cylinder varied from the nozzle exit diameter $d_{n,e} = 0.79$ cm to 2.79 cm. Finally, a 3D interaction of the nozzle plume with a plate, smooth and rough, is simulated. The computational geometry included the nozzle with the external side of the plenum and the plate which size and location correspond to the experimental setup.

The DSMC-based software system SMILE [12] was used in all DSMC computations. The important features of SMILE that are relevant to this work are parallel capability, different collision and macroparameter grids with manual and automatic adaptations, and spatial weighting for axisymmetric flows. The majorant frequency scheme was used to calculate intermolecular interactions. The intermolecular potential was assumed to be a variable hard sphere. Energy redistribution between the rotational and translational modes was performed in accordance with the Larsen-Borgnakke model. A temperature-dependent rotational relaxation number was used. The reflection of molecules on the surface was assumed to be

diffuse with complete energy and momentum accommodation.

All walls were assumed to be at a temperature of 300 K, except where specified otherwise, and the propellant gas is nitrogen at a stagnation temperature of 300 K. A background pressure of zero was assumed in all calculations. In the first series of computations (nozzle plume expansion into a vacuum) the computational domain included a part of the plenum large enough to avoid the impact of the domain size on the results, and the total number of collision cells and molecules was about 400,000 and 4 million, respectively. For the axisymmetric interaction of a plume with a hollow cylinder these numbers were 1.5 and 8 million, respectively. The three-dimensional plume-surface interaction was modeled using a starting surface at the nozzle exit, generated using an axisymmetric solution of a nozzle plume expansion. An elliptic distribution function was used for inflow molecules. The number of simulated molecules and cells was about 20 million and 3 million, respectively.

4   Nozzle Surface Roughness

A close examination of the surface structure inside the actual nozzle manifested a very rough, groove-like structure, as illustrated in Fig. 2, with micron-size grooves set out perpendicular to the main flow direction. The evident surface roughness prompted the authors to numerically study the effect of roughness inside the nozzle on the nozzle thrust. To this end, axisymmetric DSMC computations were performed for a rough surface of the diverging part of the nozzle, assumed to have a regular triangular, saw-tooth structure with the triangle angle of 90 deg, and the distance between the triangles of 10μm. The diffuse model of reflection with full energy and momentum accommodation was used on triangle surfaces. A total of more than 1,000 was used, and the results are compared with those obtained for a flat diffusely reflecting surface (called "smooth" hereafter).

The comparison of number density fields inside a rough and a smooth nozzles is presented in Fig. 3 for the smallest chamber pressure considered, $P_0 = 18$ Pa. The figure also illustrates the geometry of the nozzle and the computational domain. The results show that the influence of the surface roughness in the diverging part propagates into the plenum, and the density for the rough surface is about 10% lower than the corresponding values inside the smooth nozzle. This is easily explained by the fact the the flow is subsonic in the most part of the nozzle, and becomes supersonic only near the exit. The difference between rough and smooth is larger near the surface than at the centerline, and amounts to almost 20% at

the nozzle lip. The larger density for the rough case is explained by a significant amount of molecules reflected on the windside of the triangles and traveling toward the throat.

The molecules reflected on the windside of triangles increase density and decrease axial velocity in the diverging part of the nozzle. This decrease in axial velocity, however is compensated by the contribution molecules reflected on the triangle lee sides, that on average are reflected in axial direction. The combined effect of these two trends results in a small influence of the surface roughness on the axial flow velocity fields, as shown in Fig. 4. Although there is a visible difference near the nozzle surface, with the rough case values at the surface being lower by over 50m/s, the profiles at the nozzle exit are close.

The quantitative impact of the surface roughness inside the nozzle on the flow properties is given in Table 1, where the nozzle performance properties are shown for three plenum pressures. As expected, the effect of roughness is maximum at the lowest pressure, with the rough case mass flow being over 12% lower than the corresponding smooth case. Since the axial velocity at the nozzle exit is weakly affected by the surface roughness, the thrust force is also about 12% lower, and the specific impulse does not change with roughness. For a ten times larger pressure, $P_0 = 180$ Pa, the surface roughness causes only a 3% decrease in the mass flow and, again, practically no change in the specific impulse. At an even higher pressure of 1,800 Pa, no visible influence of the nozzle roughness was found.

The conclusion from these computations is that the surface roughness in the nozzle impacts mostly the density fields; its effect on the axial velocity is much smaller. Correspondingly, the mass flows is significantly reduced by the surface roughness only for throat-based Reynolds numbers of about unity or lower, when the subsonic region occupies large part of the diverging part of the nozzle. The surface roughness was found to have little effect on the specific impulse. All this also shows that the experimental data on plume and surface forces shown below as function of the mass flow rate is not affected by the nozzle surface roughness.

5   Axisymmetric
Plume-Surface Interaction

The study of the plume-surface interaction with different roughness structure has been started with an axisymmetric nozzle-hollow cylinder geometry. The axisymmetric geometry was selected due to the relative simplicity of the flow as well as numerical effi-

ciency compared to a 3D plume-surface interaction. A plume from the nozzle is directed into a cylinder with the axis coinciding with the plume axis, and a diameter varying from $d_{n,e}$ to $d_{n,e} + 8$ mm, where $d_{n,e}$ is the nozzle exit diameter. A plenum pressure of 1800 Pa was used in all calculations presented in this section.

The first configuration considered is shown in Fig. 5, where the pressure fields are given for a smooth (diffuse reflection) and rough (triangular roughness shape) cylinders. The larger distance between the triangles of 0.001 mm was used for the roughness characteristic size to be on the order of or larger than the gas mean free path. Note that the starting surface was used in these computations, with the inflow boundary located in the middle of the diverging part of the nozzle, and the inflow parameters taken from the full nozzle modeling with a smooth surface.

The most important conclusion here is the surface roughness does not have a pronounced effect on gas pressure. Pressure is one to three percent high for the rough case, with qualitatively the same flow structure. Initially, the pressure drops in the nozzle. Then, there is a pressure increase in the center of the cylinder part due to the formation of the viscous layer at the cylinder surface. Even a smaller difference between the rough and smooth cases is observed for the axial flow velocity fields presented in Fig. 6. Although there is a minor difference near the surface, with the velocity somewhat lower near the rough cylinder, the velocity near the axis is practically not affected by the surface roughness.

This behavior is similar to that inside the nozzle shown in the previous section. The molecular explanation of this effect given for the low-pressure gas flow inside the nozzle is however not applicable for this case of a relatively high pressure. The gas mean free path inside the cylinder is about 10^{-4} m, which corresponds to the roughness size based Knudsen number of about 0.1, and the cylinder diameter based Knudsen number of about 0.01. The flow is therefore near-continuum; the gas stagnates inside the triangular cavities of the rough surface, and acts as a pseudo-surface in terms of flow development. As a result, the cavities do no significantly affect the flow.

This is also illustrated in Fig. 7 where the pressure fields are shown for rectangular and triangular roughness shapes. The roughness shape does not impact the flow, and the determining factor in this case is the minimum cylinder diameter and not the roughness type. The results do no change when deeper cavities are used for the rectangular roughness shape.

The next configuration considered is that with a larger diameter of the cylinder, $d_{n,e} + 8$ mm. In this case, the density inside the cylinder is significantly smaller, and the cylinder diameter based Knudsen number is about 0.1. The pressure and axial velocity fields for the larger cylinder diameter case are shown in Figs. 8 and 9. There is a local pressure maximum inside the cylinder, although less pronounced than for the smaller diameter of the cylinder. The flow inside the nozzle is weakly affected by the cylinder. Most important, the gas pressure is not influenced noticeably by the surface roughness. The axial velocity is also not affected by the roughness.

In order to understand the effect of the surface roughness that might be obtained in the experimental setup used in this work, it is necessary to compute axial forces on the cylinder, and compare them to the thrust forces from the nozzle. The computed values of the axial force for three different diameters of the cylinder are listed in Table 2. Here, d is the difference between the cylinder and nozzle exit diameters. The total axial force on the cylinder is comparable with the thrust force of 0.178×10^{-2} N. The difference between the smooth and rough surfaces is small, though. It is within the statistical error of the computations for $d = 0$, and slightly increases for larger cylinders. However, even for $d = 8$ mm it amounts to about percent of the total nozzle thrust, making it practically impossible to characterize experimentally.

The computations were performed up to $d = 20$ mm, when the gas mean free path near the surface is significantly larger than the roughness size; no considerable effect of roughness on the axial force was found. This is somewhat counter-intuitive: although the incident plume particles have same contribution to the axial force both for smooth and rough surfaces, the reflected molecule contribution on rough surface is expected to be a finite number, compared to zero for the smooth surface. The small difference between rough and smooth surfaces in the near-free molecular regime is because for the cylindrical geometry many molecules that reflect from the surface collide with the opposite side of the cylinder. Among all particles that collide with the surface, the number of particles that experience such multiple reflections is greater than those that come directly from the plume, and therefore the effect of surface roughness is minimized.

The effect of multiple reflections of particles on the surface decreases with the decrease of the cylinder length. The axial force values for a plume impinging on a short cylinder of a length 5 mm given in Table 2 show that there is a 12% difference between the smooth and rough cylinders. The absolute magnitude of this difference is small compared to the nozzle thrust force, though. This makes the shorter cylinder case difficult to examine experimentally. The pressure field for the shorter cylinder is presented in

Fig. 10. Pressure inside the cylinder is noticeably higher for the rough cylinder. The difference in flow velocities is smaller than that in pressures, though.

The computations were also performed for an elevated surface temperature inside the cylinder, and showed that the smooth/rough surface difference increases with temperature. For a surface temperature of 600 K the axial force on the rough cylinder is about 5% larger than that for a smooth one. Generally, the computations of a plume interacting with the inner surface of a cylinder allow us to conclude that the surface roughness has relatively small effect on flow fields and surface forces, and this effect is too small to be studied experimentally. The shorter cylinder computations show that the effect should be significant in a 3D case of a plume interacting with a flat surface. This case is considered in the following section.

6 Interaction of Plume with a Plate: Numerical Modeling

Consider now the 3D interaction of a rarefied plume with a plate. The pressure flow field in the plane perpendicular to the plate surface and coming through the nozzle axis is given in Fig. 11 for a smooth plate and the stagnation pressure of 405 Pa. The interaction region between the plume and the plate is clearly seen, with the local pressure maximum located near the plate surface about 6 mm downstream from the nozzle exit plane. The pressure values in that region are over an order of magnitude larger than those at the corresponding location in the bottom half of the plume. There is significant backflow observed as the result of the plume-surface interaction. A strong backflow will result in a contribution of backflow molecules interacting with the plenum surface to the total force. This contribution increases the total force in x-direction.

The flow does not change qualitatively when a plate with a triangular surface roughness is used (see Fig. 12). Quantitatively, however, the pressure maximum at the plate shifts about 1 mm downstream compared to the smooth surface case, and the maximum value increases by about 10%. The pressure is generally higher for the rough plate, since most of the plume molecules that collide with the surface are reflected backwards for that case. This is especially noticeable in the back flow region where the pressure for the rough surface case is about two times higher. Note that the mean free path of the gas near the plate is on the order of 1 cm, and is an order of magnitude larger that the roughness size.

In addition to the triangular groove roughness, a rectangular grove shape has also been examined. The pressure for the latter case is somewhat lower than for the triangular one, but is still higher than for the smooth surface, as shown in Fig. 13.

The increase in the angle of the plate measured from the plume direction from 0 to 10 deg significantly weakens the plume-surface interaction, as shown in Fig. 14. The pressure maximum is more than two times smaller for 10 deg than it was for 0, and the plate no longer has a noticeable effect on the flowfield in the immediate vicinity of the nozzle exit. The backflow pressure is also reduced and is only slightly higher than the corresponding pressure at the bottom half of the plume backflow. The effect of the plate surface roughness on the pressure field for 10 deg is similar to that for 0 deg, and is not shown here.

Consider now the effect of the plume roughness on surface forces. The distribution of the forces in X direction (shear force) and Y direction (pressure force) over a smooth plate is shown in Figs. 15 and 16. Here, X direction coincides with the direction of the plume, and Y direction is perpendicular to the plate surface. The maximum in F_x force of about 0.26 N is located close to the plate center, in the region where both molecular density and axial velocities are sufficiently large. The maximum in F_y force is shifted a few millimeters to the nozzle exit plane, where the local gas pressure maximum is observed. The maximum F_y is about two times larger than the corresponding maximum F_x, primarily because the force from reflected molecules is finite for F_y and zero for F_x. Also, the axial velocity component of plume molecules in that region is somewhat larger than the radial one, with the incidence angle typically larger than 45 deg.

The next two figures, Figs. 17 and 18, present the corresponding force distributions for a rough surface of the plate (triangular roughness). It is clearly seen the discontinuous structure of the force distributions. The F_x values are large on the sides of the grooves directed toward the nozzle (windside), with the maximum value almost three times larger than the corresponding maximum on a smooth plate. The lee sides of the grooves however are characterized by forces that act in the direction opposite to the plume direction, therefore reducing the large force from the wind sides. The maximum value of F_x on a rough plate is close to that of F_y. The wind-lee side structure of the surface is also clearly seen in F_y, although the direction of the forces is the same for this case.

The forces on the plate F_x and F_y and on the plenum surface F_b are presented in Table 3 for two roughness types and two angles of the plate. For the plate angle of 0 the magnitude of the forces on the plate is comparable to the plume thrust force F_{th}, with F_x and F_y being about 25% and 30% of

the thrust, respectively. Comparison of rough and smooth surfaces shows that the magnitude of F_x is the smallest for the smooth plate and largest for a plate with the triangular roughness shape. The difference is about 20% for these cases. The force in Y direction practically does not depend on surface roughness.

Another important contributor to the total X-force F_{tot} is the force on the plenum, primarily caused by molecules reflected on the plate. This force is significantly larger for rough plates, with the value for the triangular roughness type about 50% higher than that for the smooth plate. Since the force on the plenum is in the direction opposite to that on the plate, this 50% difference considerably reduces the effect of surface roughness on F_tot. The difference between F_{tot} for a smooth and a rough plate with triangular grooves amounts to only about 3% of the total force. For the angle of 10 deg, this difference is only about 2.5%.

The comparison of contributions to the total force for a plume flow at $P_0 = 155$ Pa, interacting with smooth and rough surfaces, is given in Table 4. As compared to $P_0 = 405$ Pa, all forces scale approximately with the stagnation pressure, and the conclusion made for the higher pressure case are applicable for $P_0 = 155$ Pa.

7 Interaction of Plume with a Plate: Experimental Study

Comparison of computed and measured total forces versus mass flow is presented in Fig.19. Here, the lines that show numerical solution were created using the values of F_{tot} listed in Tables 3 and 4, that correspond to the chamber pressures of 155 and 405 Pa. The agreement between the experimental and computed force values is good, and the difference in all cases does not go beyond a few percent. The experimental and numerical forces practically coincide both for a smooth polished plate and a rough plate with triangular roughness. The values for a plate with rectangular grooves are closer to those for a smooth plate in DSMC, and to triangular grooved plate in the experiment, although the difference is rather small and may be attributed to one or several causes of experimental and numerical inaccuracies.

There are several possible sources of experimental uncertainties in this work. First, there is always a finite background gas pressure in the chamber that increases with mass flow. The background gas may impact the mass flow measurements only for plenum pressures larger than 10 torr, although the force (momentum flux) measurements are affected to some ex-

tent at all plenum pressures. A previous study [13] indicated that the force can be effected by less than 0.5% at the experimental conditions of this work. A stand calibration of deflection angle vs applied force has been approximated to be within 3%. For a given applied force to the stand, the standard deviation of the stand's deflection was less than 1%; however, the accuracy of the calibration system must also be taken into account. Finally, there was some error associated with the manufacturing of the nozzle. The nozzle throat diameter is known only with an accuracy of 1%, and the nozzle surfaces are significantly rough. As was mentioned above, the effect of these last issues are minor for the presented results. In addition to the experimental uncertainties, there are a number of numerical uncertainties. Grid resolution, the maximum number of simulated molecules, effects of the subsonic boundary conditions, and the gas-gas collision models all account for a numerical uncertainty estimated to be on the order of 1 to 2%.

The experimental results for a wider range of mass flows that correspond to plenum pressures up to about 17 torr are shown in Fig. 20. The addition of an engineering plate significantly reduces total force, up to 15%. The surface roughness effect is much smaller, and the effect of the roughness type is negligible. The small difference between rough and smooth surfaces is explained by the effect of the plume molecules colliding with the plenum, as discussed in the previous section.

8 Conclusions

Experimental and numerical modeling of a cold gas nozzle plume interacting with engineering surfaces is performed for nitrogen propellant in the range of nozzle throat based Reynolds numbers from about 2 to 600. A nano-Newton resolution force balance was used in the experimental study to measure thrust force of a plume expanding from a conical nozzle, and then the total force resulted from the interaction of the plume with aluminum plates attached to the same force balance. Smooth and rough plates were examined, with surface roughness introduced through a set of equally spaced 0.5 mm wide grooves perpendicular to the flow direction.

The DSMC method was used in the numerical study, with the setup corresponding to that in the experiment. The calculated force vs mass flow was found to be in a good agreement with the corresponding experimental data. The experiments and computations showed that there is significant thrust degradation due to the plume surface interaction, with the total decrease being up to 15%. The force on the plate increases in magnitude by about 20% for the rough

6

surface as compared to the smooth one. However, the impact of the surface roughness on total force is small, which is attributed primarily to the effect of plume molecules reflected from the plate backwards to the plenum surface. The number of such molecules is significantly larger for rough surfaces.

The impact of the surface roughness inside the nozzle has been studied numerically. It was shown that the surface roughness decreases both mass flow and thrust by over 10% for Reynolds numbers on the order of one. The effect decreases with the increase of the Reynolds number, and is negligible at Re > 100. The specific impulse is not affected by the surface roughness even at small Reynolds numbers.

9 Acknowledgements

References

[1] Boyd, I. and Ketsdever, A., "Interactions Between Spacecraft and Thruster Plumes," *J. Spacecraft and Rockets*, 38, 380 (2001).

[2] Lengrand, J-C., Allegre, J., Bisch, D., Skovorodko, P., "Impingement of a Simulated Rocket Exhaust Plume onto a Surface," in Rarefied Gas Dynamics - Proceedings of the 20th International Symposium, edited by C. Shen, Bejing University Press, Beijing, 1997, pp. 537-542.

[3] Ivanov, M., Markelov, G., Kaskhovsky, A., Giordano, D., "Numerical Analysis of Thurster Plume Interaction Problems," in Proceedings of Second European Spacecraft Propulsion Conference, ESA SP-38, 1997, pp. 603-610.

[4] Hyakutake, T., Nishida, M., "Numerical Simulation of Rarefied Nozzle Plume Impingements," in Rarefied Gas Dynamics, Proceedings of the 22nd International Symposium, edited by T. Bartel and M. Gallis, AIP Conference Proceedings 585, American Institute of Physics, New York, 2001, pp. 806-811.

[5] Legge, H., "Plume Impingement Forces on Inclined Flat Plates," in Rarefied Gas Dynamics, Proceedings of the 17th International Symposium, edited by A. Beylich, VCH, Aachen, 1991, pp. 955-962.

[6] Deependran, B., Sujith, R., Kurian, J., "Impingement of Low Density Freejets on a Flat Plate," in Rarefied Gas Dynamics - Proceedings of the 20th International Symposium, edited by C. Shen, Bejing University Press, Beijing, 1997, pp. 465-466.

[7] Ketsdever, A., Micropropulsion for Small Spacecraft, AIAA Progress Series in Astronautics and Aeronautics, eds. Micci and Ketsdever, Vol. 187, 2000, pp. 139-166.

[8] Jamison, A., Ketsdever, A., and Muntz, E. P., "Gas Dynamic Calibration of a Nano-Newton Thrust Stand," Review of Scientific Instruments, Vol. 73, No. 10, 2002, pp. 36293637.

[9] Ketsdever, A., "Facility Effects on Performance Measurements of Micropropulsion Systems Which Utilize Gas Expansion," Journal of Propulsion and Power, Vol. 18, No. 4, 2002, pp. 797804.

[10] Rothe, D., "Electron-Beam Studies of Viscous Flow in Supersonic Nozzles," AIAA Journal, Vol. 9, No. 5, 1971, pp. 804810.

[11] Ivanov, M., Markelov, G., Ketsdever, A., and Wadsworth, D., "Numerical Study of Cold Gas Micronozzle Flows," AIAA Paper 99-0166, Jan. 1999.

[12] Ivanov, M.S., Markelov, G.N., Gimelshein, S.F. "Statistical simulation of reactive rarefied flows: numerical approach and applications," *AIAA Paper 98-2669,* June 1998.

[13] Ketsdever, A.D.. "Facility effects on performance measurements of micropropulsion systems that utilize gas expansion," *J. Propulsion and Power,* 2002, Vol. 18, No. 4, pp. 797-804.

Table 1: Impact of surface roughness on nozzle properties.

Po, N/m^2	Surface type	Mass flow, kg/s	Thrust, N	Isp , s
$1.821 \cdot 10^3$	*Smooth*	$0.2804 \cdot 10^{-5}$	$0.1780 \cdot 10^{-2}$	$0.6475 \cdot 10^2$
$1.821 \cdot 10^3$	*Rough*	$0.2800 \cdot 10^{-5}$	$0.1770 \cdot 10^{-2}$	$0.6449 \cdot 10^2$
$1.821 \cdot 10^2$	*Smooth*	$0.2301 \cdot 10^{-6}$	$0.1176 \cdot 10^{-3}$	$0.5213 \cdot 10^2$
$1.821 \cdot 10^2$	*Rough*	$0.2226 \cdot 10^{-6}$	$0.1122 \cdot 10^{-3}$	$0.5143 \cdot 10^2$
$1.821 \cdot 10^1$	*Smooth*	$0.1548 \cdot 10^{-7}$	$0.7424 \cdot 10^{-5}$	$0.4892 \cdot 10^2$
$1.821 \cdot 10^1$	*Rough*	$0.1375 \cdot 10^{-7}$	$0.6614 \cdot 10^{-5}$	$0.4908 \cdot 10^2$

Table 2: The axial force on the cylinder for surface conditions and diameters

d, mm	Surface type	Temperature, K	Length, mm	Fx, N
0	*Smooth*	300	25.5	$0.1097 \cdot 10^{-2}$
0	*Rough*	300	25.5	$0.1080 \cdot 10^{-2}$
4	*Smooth*	300	25.5	$0.7770 \cdot 10^{-3}$
4	*Rough*	300	25.5	$0.7906 \cdot 10^{-3}$
8	*Smooth*	300	25.5	$0.7187 \cdot 10^{-3}$
8	*Rough*	300	25.5	$0.7408 \cdot 10^{-3}$
16	*Smooth*	300	25.5	$0.5889 \cdot 10^{-3}$
16	*Rough*	300	25.5	$0.6236 \cdot 10^{-3}$
8	*Smooth*	300	5.0	$0.2762 \cdot 10^{-3}$
8	*Rough*	300	5.0	$0.3101 \cdot 10^{-3}$
8	*Smooth*	600	25.5	$0.8371 \cdot 10^{-3}$
8	*Rough*	600	25.5	$0.8780 \cdot 10^{-3}$

Table 3: Surface forces for $P_0 = 405$ Pa.

Surface	Angle	F_{th}, N	$F_{x,s}$, N	$F_{y,s}$, N	$F_{b,n}$, N	F_{tot}, N
Smooth	0	$0.309 \cdot 10^{-3}$	$-0.6762 \cdot 10^{-4}$	$0.1093 \cdot 10^{-3}$	$0.1204 \cdot 10^{-4}$	$2.5342 \cdot 10^{-4}$
Rectangular	0	$0.309 \cdot 10^{-3}$	$-0.7340 \cdot 10^{-4}$	$0.1083 \cdot 10^{-3}$	$0.1519 \cdot 10^{-4}$	$2.5079 \cdot 10^{-4}$
Triangular	0	$0.309 \cdot 10^{-3}$	$-0.8256 \cdot 10^{-4}$	$0.1124 \cdot 10^{-3}$	$0.1808 \cdot 10^{-4}$	$2.4452 \cdot 10^{-4}$
Smooth	10	$0.309 \cdot 10^{-3}$	$-0.3076 \cdot 10^{-4}$	$0.7252 \cdot 10^{-4}$	$0.5641 \cdot 10^{-5}$	$2.8388 \cdot 10^{-4}$
Triangular	10	$0.309 \cdot 10^{-3}$	$-0.4059 \cdot 10^{-4}$	$0.7481 \cdot 10^{-4}$	$0.9040 \cdot 10^{-5}$	$2.7745 \cdot 10^{-4}$

Table 4: Surface forces for $P_0 = 155$ Pa.

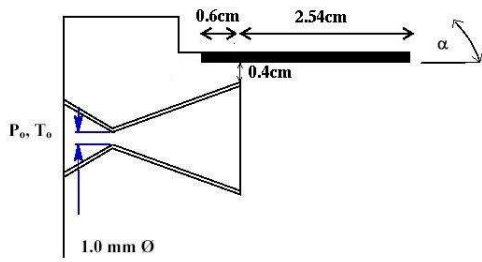| Surface	Angle	F_{th}, N	$F_{x,s}$, N	$F_{y,s}$, N	$F_{b,n}$, N	F_{tot}, N
Smooth	0	$0.949 \cdot 10^{-4}$	$-0.2368 \cdot 10^{-4}$	$0.3799 \cdot 10^{-4}$	$0.4618 \cdot 10^{-5}$	$0.7584 \cdot 10^{-4}$
Rectangular	0	$0.949 \cdot 10^{-4}$	$-0.2595 \cdot 10^{-4}$	$0.3770 \cdot 10^{-4}$	$0.6036 \cdot 10^{-5}$	$0.7499 \cdot 10^{-4}$
Triangular	0	$0.949 \cdot 10^{-4}$	$-0.2960 \cdot 10^{-4}$	$0.3822 \cdot 10^{-4}$	$0.7315 \cdot 10^{-5}$	$0.7262 \cdot 10^{-4}$

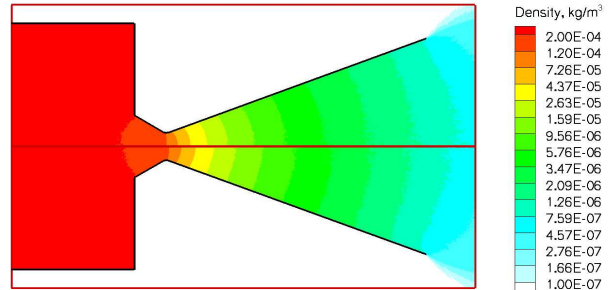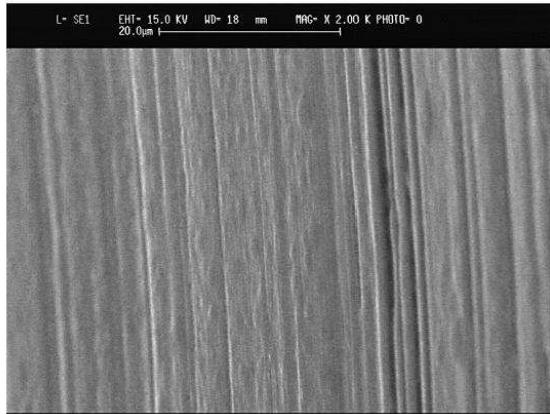Figure 1: Schematic of the geometric setup in the experiment.

Figure 2: Scanning electron microscope image showing the surface roughness of the expanding section of the conical nozzle.

Figure 3: Comparison of the mass density fields for a smooth and rough nozzles.
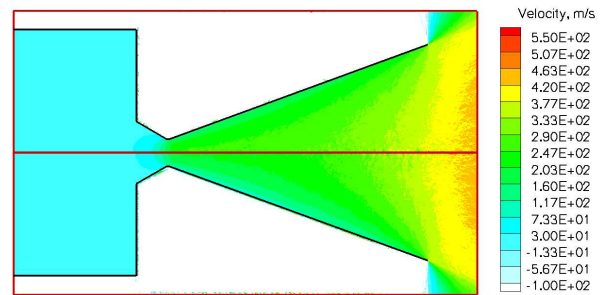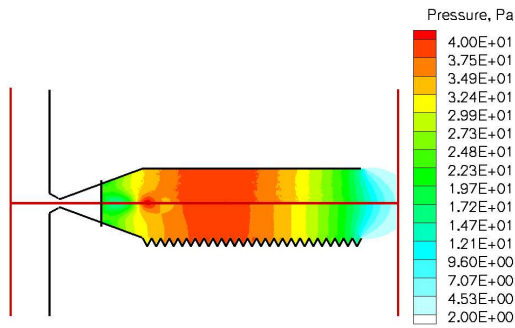

Figure 4: Comparison of the axial velocity fields for a smooth and rough nozzles.

9

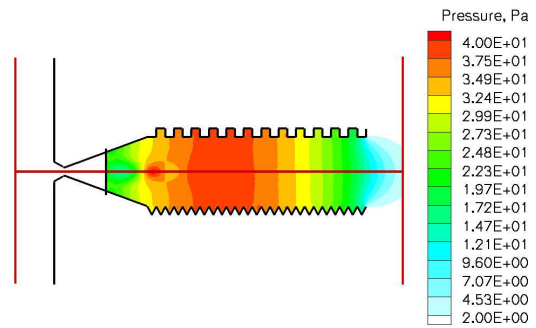Figure 5: Comparison of the pressure fields for smooth and rough cylinders with the inner diameter of 0.79 cm.

Figure 7: The impact of the roughness shape on pressure fields for the plume-cylinder interaction. Cylinder diameter is 0.79 cm.
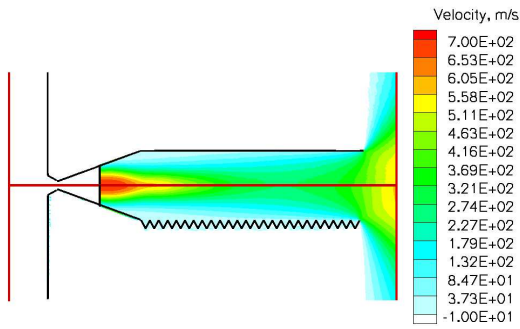
Figure 6: Comparison of the axial velocity fields for smooth and rough cylinders with the inner diameter of 0.79 cm.
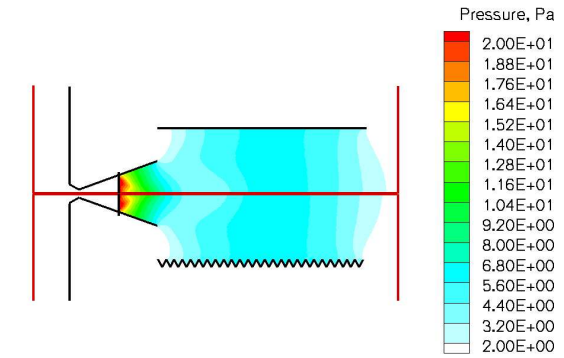
Figure 8: Comparison of the pressure fields for smooth and rough cylinders with the inner diameter of 1.59 cm.

Figure 11: Pressure field (Pa) over a smooth plate at 0 deg.

Figure 9: Comparison of the axial velocity fields for smooth and rough cylinders with the inner diameter of 1.59 cm.
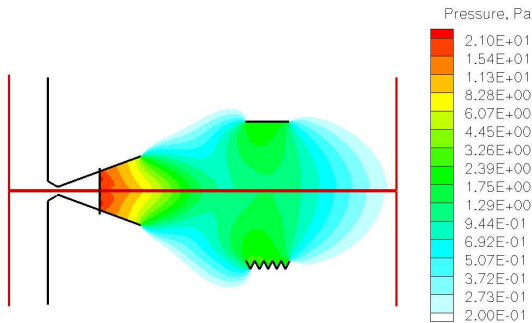
Figure 10: Comparison of the pressure fields for 5 mm long rough and smooth cylinders with the inner diameter of 1.59 cm.
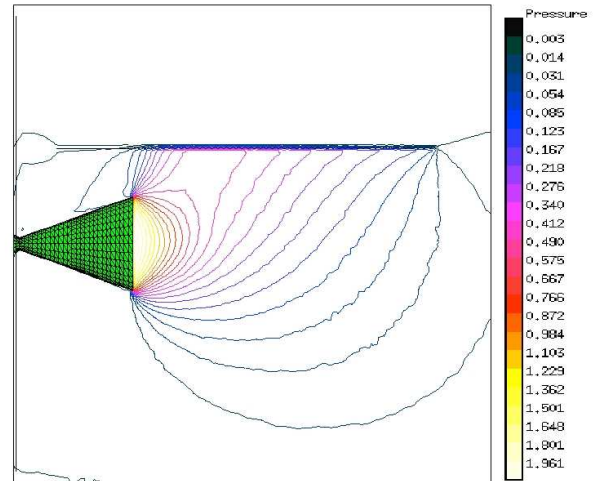
Figure 12: Pressure field (Pa) over a rough plate with triangular grooves.
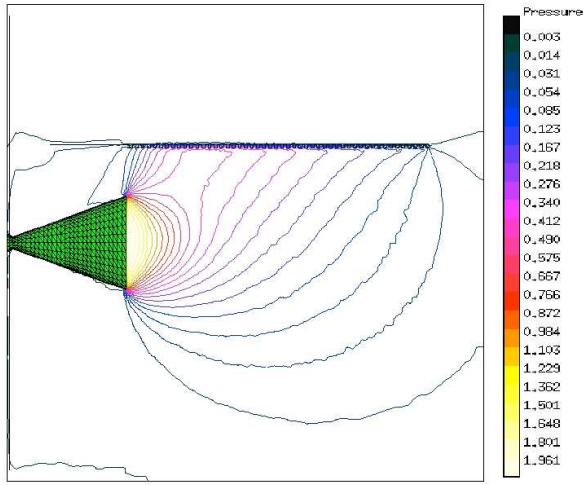
Figure 13: Pressure field (Pa) over a rough plate with rectangular grooves.
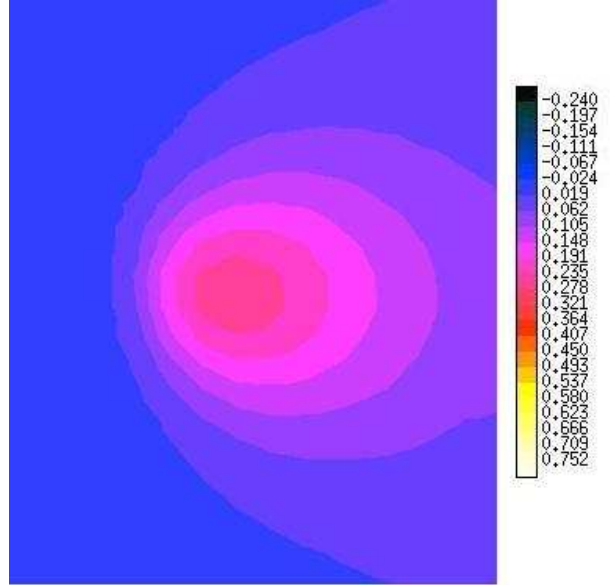
Figure 15: Force in X direction per unit area (N/m^2) on a smooth plate for the plate angle of 0 and $P_0 = 405$ Pa.
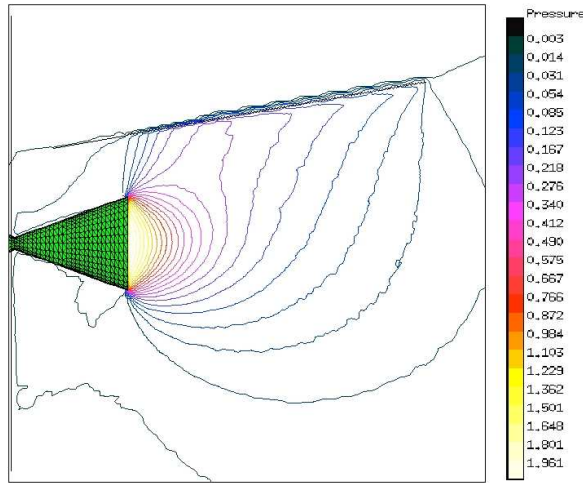
Figure 14: Pressure field (Pa) over a rough plate with triangular grooves. Plate angle is 10 deg.
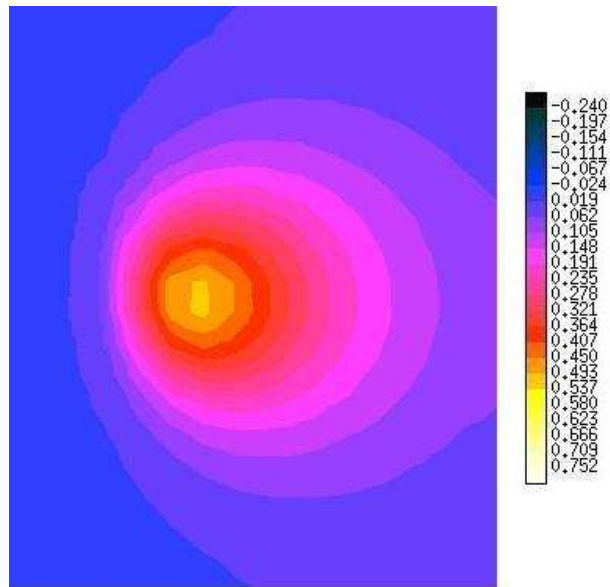
Figure 16: Force in Y direction per unit area (N/m^2) on a smooth plate for the plate angle of 0 and $P_0 = 405$ Pa.
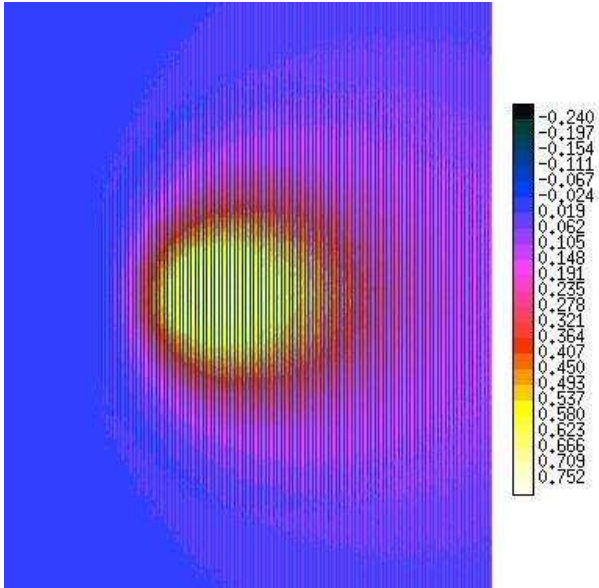
Figure 17: Force in X direction per unit area (N/m²) on a rough plate for the plate angle of 0 and $P_0 = 405$ Pa.
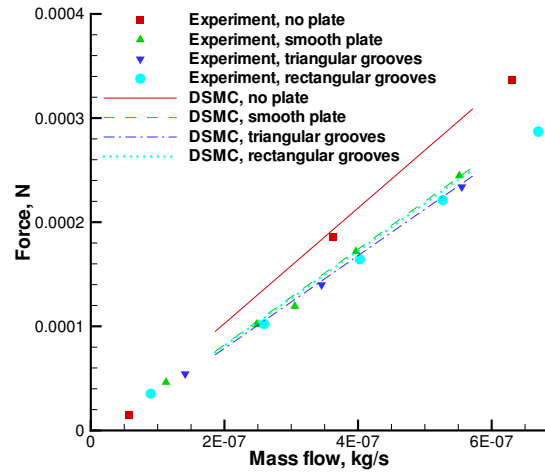

Figure 19: Total force versus mass flow for free expansion and smooth and rough surfaces: comparison of numerical and experimental modeling.
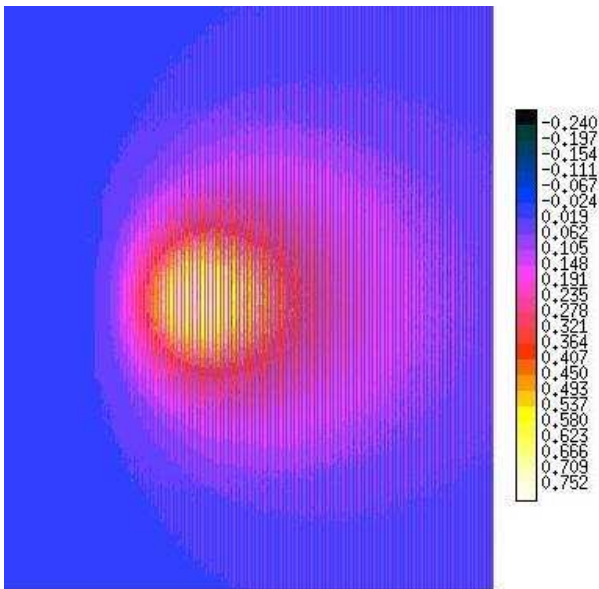

Figure 18: Force in Y direction per unit area (N/m²) on a rough plate for the plate angle of 0 and $P_0 = 405$ Pa.
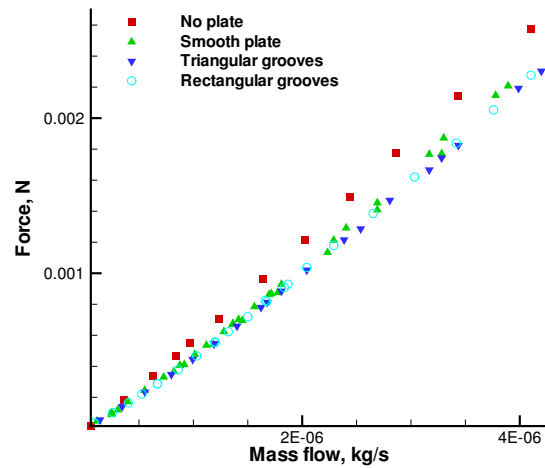

Figure 20: Measurements of total force versus mass flow for free expansion and smooth and rough surfaces.